HHS Public Access

Author manuscript

Neurobiol Dis. Author manuscript; available in PMC 2017 January 01.

Published in final edited form as:

Neurobiol Dis. 2016 January ; 85: 130–143. doi:10.1016/j.nbd.2015.10.003.

Oxidative stress and mitochondria-mediated cell death mechanisms triggered by the familial Danish dementia ADan amyloid

Krysti Todd[a], **Jorge Ghiso**[a,b,§,*], and **Agueda Rostagno**[a,§,*]

[a]Department of Pathology, New York University School of Medicine, New York, NY, 10016, USA

[b]Department of Psychiatry, New York University School of Medicine, New York, NY, 10016, USA

Abstract

Familial Danish Dementia (FDD), an early-onset non-amyloid-β (Aβ) cerebral amyloidosis, is neuropathologically characterized by widespread cerebral amyloid angiopathy, parenchymal amyloid and preamyloid deposits, as well as neurofibrillary degeneration indistinguishable to that seen in Alzheimer's disease (AD). The main amyloid subunit composing FDD lesions, a 34-amino acid de-novo generated peptide ADan, is the direct result of a genetic defect at the 3'-end of the *BRI2* gene and the physiologic action of furin-like proteolytic processing at the C-terminal region of the ADan precursor protein. We aimed to study the impact of the FDD mutation, the additional formation of the pyroglutamate (pE) posttranslational modification as well as the relevance of C-terminal truncations –all major components of the heterogeneous FDD deposits–on the structural and neurotoxic properties of the molecule. Our data indicates that whereas the mutation generated a β-sheet-rich hydrophobic ADan subunit of high oligomerization/fibrillization propensity and the pE modification further enhanced these properties, C-terminal truncations had the opposite effect mostly abolishing these features. The potentiation of pro-amyloidogenic properties correlated with the initiation of neuronal cell death mechanisms involving oxidative stress, perturbation of mitochondrial membrane potential, release of mitochondrial cytochrome c, and downstream activation of caspase-mediated apoptotic pathways. The amyloid-induced toxicity was inhibited by targeting specific components of these detrimental cellular pathways, using reactive oxygen scavengers and monoclonal antibodies recognizing the pathological amyloid subunit. Taken together, the data indicate that the FDD mutation and the pE posttranslational modification are both primary elements driving intact ADan into an amyloidogenic/neurotoxic pathway while truncations at the C-terminus eliminate the pro-amyloidogenic characteristics of the molecule, likely reflecting effect of physiologic clearance mechanisms.

[*]Correspondence should be addressed to: Agueda A. Rostagno, Ph.D., New York University School of Medicine, 550 First Avenue, MSB Room 556, New York, NY 10016, USA. Tel: +1 212 263 6583; agueda.rostagno@nyumc.org or Jorge A. Ghiso, Ph.D., New York University School of Medicine, 550 First Avenue, MSB Room 556, New York, NY 10016, USA. Tel:+1 212 263 7997; jorge.ghiso@nyumc.org.

[§]Both authors contributed equally

Keywords

familial Danish dementia; cerebral amyloidosis; oligomeric amyloid assemblies; apoptosis; cytochrome c; oxidative stress

Introduction

Familial Danish Dementia (FDD) is a rare autosomal dominant, early-onset neurodegenerative disorder. Also termed heredopathia opthalmo-oto-encephalica [1], the disease is clinically characterized by cataracts, deafness, progressive ataxia, and dementia. Cataracts are typically the first manifestation of the disease, developing before the age of 30, followed by hearing loss about 10-20 years later and cerebellar ataxia shortly after the age of 40. Paranoid psychosis and severe dementia appear after the age of 50, whereas the median age of death is 58 years [1, 2]. Neuropathologically, FDD is characterized by brain atrophy, diffuse parenchymal preamyloid and amyloid lesions in nearly all areas of the central nervous system (CNS), occasional compact plaques, widespread amyloid angiopathy, and hippocampal neurofibrillary degeneration strikingly similar –if not identical–to that seen in Alzheimer's disease (AD) [3, 4]. Amyloid deposition in retinal blood vessels and parenchyma has been linked to retinal neovascularization leading to vitreous hemorrhage, and neovascular glaucoma [2, 4]. Despite widespread amyloid angiopathy in the small blood vessels and capillaries of the cerebrum, choroid plexus, and cerebellum, cerebral hemorrhage is rare.

FDD results from a mutation in the coding region of the *BRI2* gene located in the long arm of chromosome 13. *BRI2* normally encodes a 266-amino acid type II transmembrane protein (BRI2) of currently undefined biological function that is physiologically cleaved by furin-like proteolytic processing at peptide bond Arg^{243}-Glu^{244} to generate a 23-amino acid C-terminal peptide, Bri1-23 [5, 6] that is a normal component of cerebrospinal fluid (CSF) [7, 8]. In individuals affected with FDD, a 10-nucleotide duplication insertion (TTTAATTTGT) between codons 265 and 266, immediately before the stop codon 267, produces a shift that renders the stop signal out of frame and originates a longer than normal precursor protein with a C-terminal segment that does not exist under normal conditions (**Figure 1**). This 277-residue precursor protein, ADanPP, also undergoes furin-like proteolytic processing at the same Arg^{243}-Glu^{244} position as the non-mutated BRI2 to generate a 34-residue amyloidogenic peptide ADan [3], a molecular mechanism that is shared by a different mutation also affecting the *BRI2* stop codon and associated with a similar cerebral amyloidosis –familial British Dementia (FBD)–linked to the deposition of amyloid ABri [9].

The use of specific antibodies recognizing the unique C-terminus of ADan confirmed that vascular and parenchymal lesions in available FDD autopsy cases are primarily composed of ADan [3, 4, 10]. Parenchymal deposits co-localized with dystrophic neurites and were observed in areas most severely affected by neurofibrillary tangles [4]. Analysis of ADan species extracted from amyloid and preamyloid deposits revealed significant biochemical heterogeneity that includes N- and C- terminal truncations as well as post-translational pyroglutamate (pE) formation. Notably, the ADan molecules found in plasma were devoid

of the posttranslational modification [10] suggesting that either the formation of N-terminal pE takes place at the site of deposition or that due to the high insolubility and tendency to aggregate ADan pE species are completely deposited in the brain and systemic lesions characteristic of the disease soon after their generation disappearing from the circulation. Consistent with the higher insolubility conferred by the pE-modification, the concentration of the pE-modified species becomes more prominent as the solubility of the deposits decreases. In fact, formic acid extracts – containing the more insoluble material – are composed of heavily oligomerized ADan species, partially degraded at their N- and C-terminal ends , and almost fully modified to pE at the N-terminus [10, 11]. The truncated ADan species present in the deposits include peptides cleaved at the N-terminus –between Ala^{2}-Ser^{3}– as well as at the C-terminus –at peptide bonds Asn^{28}-Ser^{29} and His^{33}-Tyr^{34}–with ADan1-28 being the most prominent truncated fragment [10]. The formation of N-terminal pE has also been reported in AD for truncated forms of Aβ, specifically $Aβ_{pE3}$ and $Aβ_{pE11}$. The loss of one negative charge incurred by this posttranslational modification results in an increase in β-sheet content, greater hydrophobicity, and enhanced aggregation propensity of the molecule, with N-terminal cyclation providing additional resistance to proteolytic degradation [12, 13]. Indeed, it has been demonstrated that N-terminal modified species progressively accumulate in the brain at the earliest stages of AD even before the appearance of clinical symptoms suggesting that they may constitute potential seeding elements and play an important role in the formation of pathological amyloid aggregates [14]. The structural alterations introduced by the N-terminal cyclation correlate with the increased toxicity displayed when compared to full-length Aβ, further supporting the importance of this modification for the mechanism of disease pathogenesis and providing additional targets for therapeutic interventions [15-20]. Puzzlingly, biochemical and immunohistochemical analysis of FDD lesions also revealed limited co-deposition of full-length Aβ42 and N-terminally truncated Aβ4-42 within vascular and perivascular ADan deposits and occasionally in parenchymal preamyloid deposits, albeit accounting for less than one-tenth of the total deposited amyloid [4, 10]. Whether this co-deposition plays any role in the disease pathogenesis or simply reflects a conformational mimicry remains undetermined.

Previous studies with full-length ADan stressed the propensity of the molecule for oligomerization and suggested that certain amyloidogenic and cytotoxic properties of the peptide were further enhanced by the presence of N-terminal pE [21-28]. The present work provides insight into the structural properties of ADan and its C-terminally truncated derivatives, highlighting the relevance of the mutation and the pE post-translational modification in the induction of structural changes, enhancement of intrinsic pro-amyloidogenic properties, and generation of reactive oxygen species (ROS) and mitochondria-mediated cell death mechanisms, all intertwined features relevant for the disease pathogenesis.

Methods

Peptide synthesis

Synthetic homologues of ADan pE/E, ADan1-28 pE, and Bri1-23 pE/E **(Figure 1, bottom panel)** were custom-synthesized using *N-tert*-butyloxycarbonyl chemistry at ERI Amyloid Laboratory (Oxford, CT) and purified by reverse phase-high performance liquid chromatography on a Vydac C4 column (Western Analytical, Murrieta, CA). Molecular masses were corroborated by matrix-assisted laser desorption ionization time-of-flight (MALDI-TOF) mass spectrometry, and concentrations were assessed by amino acid analysis, as previously reported [29].

Circular dichroism spectroscopy

Prior to use, all synthetic homologues were incubated at a concentration of 1 mg/ml in hexafluoroisopropanol (HFIP; Sigma Chemical Co., St. Louis, MO), a pretreatment that breaks down pre-existing secondary structures and disrupts hydrophobic forces [30]. Due to these properties, over the last decade HFIP treatment has become a standard procedure for amyloid solubilization, providing consistency among different batches and leading to monodisperse amyloid subunit preparations, a critical initial step for controlled aggregation studies. Formation of stable α-helix structures after HFIP treatment was monitored over time until superimposed circular dichroism (CD) scans were obtained in subsequent days, typically between 3 and 4 days. To assess changes in peptide secondary structure over time at physiological salt concentrations, HFIP-pretreated peptides were lyophilized and subsequently reconstituted to 1 mM in 1% ammonium hydroxide followed by further dilution in a 10 mM phosphate buffer, pH 7.4, containing 150 mM sodium fluoride to a final concentration of 50 μM. Spectra in the far-ultraviolet light (wavelength range: 190–260 nm; band-width 1 nm; intervals 1 nm; scan rate 60 nm/min) yielded by the different peptides at various time points of aggregation (up to 2 days) were recorded at 24°C with a Jasco J-720 spectropolarimeter (Jasco Inc., Easton, MD). A 0.2 mm path quartz cell was used for the samples in HFIP, while a 1 mm path quartz cell was used for the samples in salt-containing buffer. For each sample, 15 consecutive spectra were obtained and averaged, and the baseline reading was subtracted. Results are expressed in terms of molar ellipticity ($deg \cdot cm^2 \cdot dmol^{-1}$), as previously described [29].

Electron Microscopy

The structure of the different amyloid homologues and the changes occurring upon incubation in physiological salt concentration containing buffers were assessed by electron microscopy (EM), as previously described [29]. The different synthetic homologues were pretreated and solubilized as above and allowed to aggregate for up to 24h, the longest time point in the cell culture experiments reported herein. Three μl aliquots of each of the peptide aggregation time point samples were placed onto carbon coated 400 mesh Cu/Rh grids (Ted Pella, Inc., Redding, CA) and stained with 1% uranyl acetate in distilled water (Polysciences, Inc., Warrington, PA). Stained grids were examined in a Philips CM-12 transmission electron microscope and photographed with a Gatan (4k × 2.7k) digital camera at the Image Core Facility of the Skirball Institute of Biomedical Medicine, NYU School of Medicine, as described [29, 31].

Thioflavin T binding assay

Following 3 day HFIP pretreatment and subsequent lyophilization as above, peptides were thoroughly dissolved to 10 mM in dimethyl sulfoxide (DMSO, Sigma) then diluted to 1 mM in deionized water followed by further dilution in 1X phosphate-buffered saline (PBS) to reach a 50 μM concentration. Reconstituted peptides were incubated at 37°C for up to 24 hours and binding of Bri1-23 as well as ADan homologues to thioflavin T (ThT) was monitored by fluorescence evaluation as described previously [29, 32]. Briefly, 6 μl aliquots from each peptide aggregation time point were added to 184 μl of 50 mM Tris-HCl buffer, pH 8.5, and 10 μl of freshly prepared 0.1 mM ThT (Sigma). Fluorescence was recorded for 300 s in an LS-50B spectrometer (Perkin Elmer, Waltham, MA) with a slit width of 10 nm and excitation and emission wavelengths of 435 and 490 nm, respectively [33].

Gel electrophoresis and Western blot

The degree of peptide aggregation under physiologic salt concentrations was evaluated by Western blot (WB). Peptides, pretreated and aggregated as for ThT assays were electrophoresed under denaturing conditions using 16.5% Tris-tricine SDS gels with a running buffer composed of 100 mM Tris-HCl, 100 mM Tricine, and 0.1% SDS with 200 mM Tris-HCl used as the anode buffer. Following electrophoretic separation, proteins were electrotransferred to polyvinylidene fluoride (PVDF) membranes (0.45 μm pore size; Immobilon, Millipore, Billerica, MA) at 400 mA for 2.5 h using 10 mM 3-cyclohexamino-1-propanesulfonic acid (CAPS, Sigma) buffer, pH 11.0, containing 10% (v/v) methanol. The membranes were blocked with 5% nonfat milk in Tris-buffered saline containing 0.1% Tween 20 (TBST) and incubated overnight at 4°C with a custom made rabbit polyclonal antibody recognizing the C-terminal portion of the ADan peptide (Ab 5282, 1:5,000) [34]. Membranes were immunoreacted with horseradish peroxidase (HRP)-labeled $F(ab')_2$ anti-rabbit IgG (1:5,000; GE-Healthcare, Piscataway, NJ) and developed by enhanced chemiluminescence (ECL) using the SuperSignal West Pico Chemiluminescent Substrate (Thermo Scientific, Waltham, MA, USA).

ANS binding assay

Changes in the exposure of hydrophobic residues for peptides pre-treated and aggregated as in ThT assays was evaluated by their ability to bind the fluorescent dye 8-anilinonapthalene-1-sulfonic acid (ANS; Sigma). Fifty μl from each of the 50 μM peptide aggregation time point samples were added to 200 μl PBS, pH 7.4, containing 2 μl of 7.5 mg/ml ANS dissolved in dimethyl formamide (Sigma). Spectra were recorded from 450 to 570 nm in a Perkin Elmer LS-50B spectrometer with excitation at 370 nm, slit width of 10 nm, and scan speed of 500 nm/min. For each sample, 7 consecutive scans were obtained and the maximum fluorescence values from each scan were averaged and plotted as ANS binding in arbitrary units of fluorescence [35].

Cell culture

Human neuroblastoma cells (SH-SY5Y) were obtained from the American Type Culture Collection (ATCC, Manassas, VA, USA) and maintained in DMEM medium (Mediatech, Masasses, VA) with 10% fetal bovine serum (FBS).

Phase contrast microscopy

SH-SY5Y cells were seeded at a density of 1×10^4 cells/well on 96-well plates and allowed to attach for 1 day prior to the addition of the different peptides, pretreated in HFIP, dissolved to 10 mM in DMSO, added of deionized water to 1 mM, and further diluted to 50 μM in DMEM, 0% FBS. Following 24-hour incubation, images were acquired using a Nikon Eclipse Ti microscope and analyzed using Image J (NIH, Bethesda, MD; http://rsbweb.nih.gov).

Cell death assays

The extent of apoptosis induced by the different peptide homologues was evaluated by quantitation of DNA-histone complex formation resulting from DNA fragmentation using Cell Death ELISA^{plus} (Roche Applied Science, Indianapolis, IN) as previously described [29, 33, 36]. SH-SY5Y cells were seeded at a density of 2×10^4 cells/well on 24-well plates and allowed to attach for 1 day prior to the addition of the respective peptide homologues at 50 μM concentration in DMEM, 0% FBS as above. Following incubation for 4 to 24 hours, plates were centrifuged to collect detached cells (Sorvall RT7, Thermoscientific; 10 min, 200 × g). Supernatants were saved for the analyses of lactate dehydrogenase (LDH) release (see below), and cells were lysed for evaluation of fragmented DNA-histone complexes (mono- and oligo-nucleosomes) following the manufacturer's instructions. For LDH quantitation, the supernatants from the peptide-treated cultures were further centrifuged to pellet any remaining cell debris (Eppendorf 5417R; 5 min, 12,000 × g), and assayed with the Cytotoxicity Detection Kit (Roche Applied Science) per the manufacturer's instructions.

1B7 Monoclonal Antibody

Various hybridoma cell lines were custom generated by fusion of myeloma cells with B cells obtained from the spleen of mice immunized with the C-terminus of ADan (CFNLFLNSQEKHY) conjugated to keyhole limpet hemocyanin (Abnova, Taipei City, Taiwan). Of the resulting clones, 1B7 (isotype IgG2a) was selected for expansion based on ELISA and WB analysis of culture supernatants. After subcloning, 1B7 hybridoma cells were grown in Protein Free Hybridoma Medium II (Life Technologies, Carlsbad, CA) and culture supernatants were subjected to chromatography on Protein G Sepharose 4 Fast Flow (GE) for purification of the monoclonal antibody according to the manufacturer's instructions. The titer of purified 1B7 was determined by ELISA using 400 ng ADan pE-coated wells and serial dilutions of the antibody (1:1,000 to 1:100,000). To examine the efficacy of 1B7 in neutralizing ADan-induced cell death, SH-SY5Y cells, seeded at a density of 10^4 cells/well on 96-well plates, were challenged with ADan pE (50 μM) in the presence or absence of 1B7 (10 ng/ml), and stained with calcein and ethidium homodimer-1 using the Live/Dead Cell Viability Assay (Life Technologies) according to the manufacturer's instructions. Images were acquired using a Nikon Eclipse Ti microscope and analyzed with Image J.

Immunocytochemical evaluation of mitochondrial cyt c subcellular localization and mitochondrial membrane potential

SH-SY5Y cells were seeded on 12 mm poly-D-lysine coated glass coverslips (BD Biosciences, Franklin Lakes, NJ) at a density of 7×10^4 cells/coverslip and allowed to attach for 1 day prior to 6 day differentiation in DMEM (Mediatech) with 10% FBS and 10 μM retinoic acid (Sigma). Cells were subsequently treated with 50 μM ADan pE or ADan E for up to 24h, fixed with 4% paraformaldehyde, and blocked with 20 mg/ml BSA in PBS containing 0.3% Triton X-100. After incubation with mouse monoclonal anti-cyt c antibody (BD Biosciences; 1:200 in PBS containing 5 mg/ml BSA, 2h at RT) followed by Alexa Fluor 488-conjugated anti-mouse IgG (Life Technologies; 1:200 in PBS with 5 mg/ml BSA, 1h at RT), nuclei were counterstained with TO-PRO-3 iodide (Life Technologies; 1:1,000) as previously described [36-38]. To examine cyt c mitochondrial localization in conjunction with changes in the membrane potential of the organelle, cells –after peptide treatment– were washed with warm PBS and incubated for 30 minutes with 1.5 μM Mitrotracker Red CM-H_2X Ros (Life Technologies), followed by cyt c immunostaining as above. All images were acquired using a Zeiss LSM 510 microscope and analyzed using Image J.

ELISA assessment of cyt c in mitochondrial and cytoplasmic subcellular fractions

Subcellular distribution of cyt c in amyloid-challenged SH-SY5Y cells was determined using mitochondrial and cytoplasmic protein extracts, prepared after subcellular fractionation essentially as described [38, 39]. Cells were seeded on 6-well plates (4×10^6 per well), allowed to rest for 1 day, and incubated in triplicate with either ADan E or ADan pE (50 μM each) for 4-24h. Cells were collected in homogenization buffer [75 mM sucrose, 225 mM mannitol, 5 mM Tris-HCl pH 7.4, containing 1 mM phenylmethylesulfonyl fluoride, and protease inhibitor cocktail (Roche)] and disrupted with the aid of a Dounce glass homogenizer. Cell homogenates were centrifuged to remove unbroken cells and nuclei (Eppendorf 5417R; 600 × g, 5 min, 4°C) and supernatants further centrifuged at 10,300 × g (5 min, 4°C) to subfractionate mitochondria. The supernatants containing the crude cytoplasmic extracts and the pellets, comprising the mitochondrial fractions were employed to quantitate cyt c by solid phase sandwich ELISA (Quantikine ELISA, human Cytochrome C Immunoassay, R & D) as described by the manufacturer. Prior to the assay, fractions containing cytoplasmic proteins were concentrated on Vivaspin 500 centrifugal concentrators (GE HealthCare, molecular weight cut off 3000), mitochondrial pellets were resuspended in Cell Lysis Buffer provided with the kit, and total protein of the respective fractions was evaluated by BCA protein assay (Thermo Fisher Scientific/Pierce). Samples and human cyt c standards were diluted in Calibrator Diluent and incubated with microtiter wells pre-coated with a monoclonal antibody specific for human cyt c. After washing away unbound proteins, wells were further incubated with an HRP-linked monoclonal antibody anti-human cyt c, color developed with tetramethylbenzinine (TMB) peroxidase substrate, and evaluated through quantitation of the Absorbance at 450 nm. The cyt c concentration of the different samples was interpolated from the standard curve with the aid of GraphPad Prism and normalized to the protein content of the respective subcellular fractions.

Detection of reactive oxygen species

For immunofluorescence microscopy detection of ROS, SH-SY5Y cells were seeded on 96-well plates (10^4 cells/well), challenged with 50 μM ADan pE or ADan E for 2 or 4h, and further incubated at 37°C with CellROX Deep Red (5μM; Life Technologies) and Hoechst Stain (0.2 μg/ml; Immunochemistry Technologies, Bloomington, MN). After fixation in 4% paraformaldehyde images were acquired in a Nikon Eclipse Ti microscope and analyzed with Image J as above. Confirmation of IF results as well as a more quantitative evaluation of amyloid-mediated ROS generation was assessed through the use of the free radical indicator 2',7'-dichlorodihydrofluorescein diacetate (DCFDA, Life Technologies). SH-SY5Y cells, after identical 4h treatment with ADan pE and ADan E homologues as above, were loaded with the cell-permeant DCFDA (10 μM, 30 min), as described [40]. After cleavage of the acetate groups by intracellular estearases and oxidation by intracellular ROS, the sensor is converted to the highly fluorescent compound 2'7'-dichlorofluorescein. The generated fluorescence, proportional to the intracellular ROS, was evaluated in a Molecular Devices FlexStation 3 microtiter plate reader with Ex/Em wavelengths of 492–495 nm and 517–527 nm, respectively. Data are represented as percentage of the corresponding no-peptide controls.

Evaluation of caspase-3 cleavage

Assessment of caspase-3 activation in SH-SY5Y cells following challenge with ADan peptides was performed employing both immunocytochemistry and In-Cell ELISA, as follows.

Immunocytochemical analysis—SH-SY5Y cells, seeded on poly-D-lysine coated glass coverslips and differentiated with retinoic acid as above, were treated with 50 μM ADan pE or ADan E for up to 24h, fixed, and blocked as for cyt c immunocytochemistry. After incubation with antibodies recognizing the cleaved (activated) form of caspase-3 (anti-cleaved caspase-3, Cell Signaling, Danvers, MA; 1:200 in PBS containing 5 mg/ml BSA, 2h at RT) followed by Alexa Fluor 488-conjugated anti-rabbit IgG (Life Technologies; 1:200 in PBS with 5 mg/ml BSA, 1h at RT), nuclei were counterstained TO-PRO-3 iodide as above. The effect of reactive oxygen scavengers on caspase-3 activation was assessed by 2h pre-incubation with 300 μM Trolox (6-hydroxy-2,5,7,8-tetramethylchroman-2-carboxylic acid; Sigma) prior to 24h ADan challenge in the presence of identical Trolox concentration. Image acquisition and analysis was performed as above.

In-Cell ELISA—Quantification of caspase-3 activation in ADan E/pE treated cells was performed using colorimetric In-Cell ELISA (Thermo Scientific/Pierce). Briefly, SH-SY5Y cells were seeded on 96-well plates (10^4 cells per well) and incubated with 50 μM ADan E or ADan pE for different times (0.5 – 24h). Cells were subsequently fixed with 4% paraformaldehyde, permeabilized, and blocked following the manufacturer's specifications. After overnight incubation with the primary anti-cleaved caspase-3 antibody, followed by the HRP-conjugate, color was developed with TMB substrate and quantitated at 450 nm. Number of cells evaluated by Janus Green whole-cell stain was used for normalization. Inhibition of caspase-3 activation was assessed by pre-incubation with a 300 μM solution of Trolox, as above. In all cases results represent mean ± SD of triplicate experiments.

Statistical analysis

ANOVA for comparison of multiple groups with Tukey *post hoc* tests, and t-tests were performed using GraphPad Prism (GraphPad, La Jolla, CA). Values of $P \leq 0.05$ were considered significant.

Results

Structural analysis of Bri1-23 and ADan peptide variants

To generate monodisperse amyloid preparations all synthetic peptides were incubated for 3 days in HFIP to break down any pre-existing structures and disrupt hydrophobic interactions that could serve as potential seeding nuclei. As illustrated in **Figure 2A** for ADan pE, the most resistant of the subunits tested, after 3 day incubation in HFIP the peptide adopted an α-helical conformation, which remained unchanged with further pretreatment as indicated by the overlapping CD signals at 3 and 4 days. Solubilization in aqueous buffer containing physiologic salt concentration caused Bri1-23, irrespective of whether it had an N-terminal pE or E, to adopt an unordered conformation (minima at 198 nm) that remained unchanged throughout the 48h duration of the experiment (**Figure 2B)**. On the contrary, ADan pE, ADan E, and the C-terminal truncated ADan1-28 pE exhibited β-sheet rich secondary structures upon initial solubilization in physiological salt concentration buffers, conformation that persisted for the 2 days tested, as indicated by the characteristic minimum at ~215 nm (**Figure 2C)**. These peptides contained some degree of random coil conformations that were more pronounced in the case of ADan1-28 pE. Notably, the β-sheet content in ADan E increased over time while it remained fairly stable in the case of ADan pE, suggesting that the pE-modified molecule acquires its final pro-amyloidogenic conformation at a faster pace.

ThT, a dye that displays enhanced fluorescence upon binding to fibrillar and protofibrillar amyloid assemblies, was used to provide information into the oligomerization/fibrillization properties of Bri1-23 and ADan synthetic homologues (**Figure 3A**) [32, 41]. Consistent with the CD data, Bri1-23 with both E and pE N-terminal residues displayed minimal binding to ThT, whereas both ADan pE and ADan E exhibited rapid fibrillization with extremely short lag-phase and fast elongation rate, reaching a plateau after only 30 minutes of incubation in salt-containing buffer. At all-time points, the fluorescence intensity remained comparatively lower for ADan E, reaching levels ~80% those of ADan pE. The truncated peptide ADan1-28 pE behaved similarly to the Bri1-23 peptides, exhibiting low ThT binding levels that reached only ~25% of the max ADan pE value. The rapid binding of ThT by ADan pE/E correlates with the primarily β-sheet secondary structure exhibited by both molecules. The aggregation pattern of the more pro-fibrillogenic ADan pE and ADan E homologues was further examined using SDS-PAGE followed by WB analysis (**Figure 3B**). Consistent with the ThT data, ADan pE aggregated rapidly to form SDS-resistant low molecular mass oligomers – primarily dimers– that were present immediately after solubilization in aqueous buffer containing physiologic salt concentration and slowly but steadily increased in molecular mass over the 24-hour period tested. ADan E displayed a similar aggregation pattern; however the oligomers increased in size more gradually and did not reach the high molecular mass displayed by ADan pE.

Abundant evidence supports the notion that intrinsic physicochemical properties, such as hydrophobicity and charge, influence the propensity of polypeptides to form oligomeric and fibrillar species [42, 43]. ANS, a fluorescent molecular probe that exhibits an increase in fluorescence intensity and blue shift upon binding to hydrophobic peptide regions, was employed to monitor changes in the exposure of hydrophobic regions of the Bri1-23 and ADan species over time (**Figure 3C**) [41]. Bri1-23 pE and Bri1-23 E caused minimal changes in ANS fluorescence rendering fluorescent signals almost indistinguishable from the buffer blanks. Both ADan pE and ADan E produced a relevant increase and shift in ANS fluorescence although the signal intensity was higher for ADan pE than for ADan E and increased over time reaching a plateau after ~5h. Consistent with the low aggregation/ fibrillization tendency displayed by ThT binding, ADan1-28 pE produced a minimal increase in ANS fluorescence.

The formation and progression of oligomeric structures formed by the different ADan homologues was also monitored via EM. As illustrated in **Figure 4** for two different magnifications (panel A: 88,000; panel B: 144,000), upon solubilization in a water-based buffer with physiologic salt concentration ADan E assembled into globular structures 4-6 nm in diameter whereas ADan pE preparations exhibited a mixture of similar round oligomers plus short protofibrils (flexible rods <50 nm in length and similar 4-6 nm diameter); large magnification images (panel B) suggests that the round structures ensemble into a bead-like fashion to form the protofibrils, as has been described in the case of Aβ [44-46]. As time progressed, short protofibrils (20-30 nm long and similar 4-6 nm diameter) appeared in the ADan E preparation (2h), co-existing with the original globular structures whereas longer protofibrils (<120 nm) were the predominant ADan pE structures at a comparable time-point. At longer times (4-8h), protofibrillar assembles continued to grow in both preparations, reaching lengths of 60 nm for ADan E and 150 nm for ADan pE. After 24h incubation, the longest time point in our studies, aggregates of the short protofibrils were present in both ADan E and ADan pE preparations, although ADan E protofibrils appeared more loosely packed than the pE counterpart. It is interesting to note that the protofibrillar structures formed by ADan pE/E are comparable to those described in early stages of Aβ aggregation in which beaded chains of round oligomeric structures were evidenced by EM studies [44, 45]. These Aβ protofibrils, exhibiting a predominantly β-sheet conformation by CD, evolved with time into the mature amyloid fibrils [45]. Our findings demonstrating the formation of similar structures in a totally unrelated amyloid subunit suggests that the formation of intermediate protofibrillar elements is a general phenomenon in amyloid fibrillogenesis. In agreement with the ThT and ANS data, the truncated ADan 1-28 subunit only formed few globular assembles (4-8 nm in diameter) and protofibrillar structures (<20 nm after 24h incubation; panel B) whereas Bri1-23, either bearing pE or E in the N-terminus, did not form discernable structures (not shown). No classical amyloid fibrils were identified in any of the preparations within the time-frame of the experiments. Whether ADan protofibrils will transition into fibrillar components with longer incubation times or whether they will remain as the primary structure as demonstrated for the Aβ Arctic mutant which is more prone to form protofibrils than both wild type Aβ1-40 and Aβ1-42 [47], remains to be further determined. The above data clearly indicates that the elongated ADan peptide, generated as a result of the FDD mutation and released by the proteolytic action of a

furin-like physiologic processing, has a higher β-sheet content, enhanced aggregation/fibrillization propensity, and greater hydrophobicity than the Bri1-23 counterpart, pro-amyloidogenic properties that are amplified by the presence of the pE post-translational modification. Also of note is the importance of amino acids 29-34 for the pro-amyloidogenic properties of ADan, as the C-terminally truncated ADan1-28 pE is far less hydrophobic and aggregation-prone than the full-length molecule.

Neurotoxicity of ADan

The effects of Bri 1-23 and ADan species in SH-SY5Y neuroblastoma cells was examined at peptide concentrations typically used *in vitro* to examine the cell death mechanisms elicited by Aβ and BRI2 related amyloids [37, 48-50]. Previous studies assessing neurotoxicity of ADan have used significantly higher peptide concentrations (200-300 μM range) [22, 24]. In our system lower concentrations were sufficient for the elucidation of the neurotoxic pathways engaged by the molecule with minimal pro-apoptotic response in the 1-10 μM range and a relevant increase over untreated controls at 50 μM (not shown), the concentration which was therefore selected for all the cell death assays described below. Following challenge with the non-amyloidogenic Bri1-23 pE or Bri1-23 E peptides, cells maintained a morphology consistent with that seen in the control cells, characterized by round cell bodies and abundant neuronal projections as shown by phase contrast imaging (**Figure 5A**). ADan pE elicited a quite different response, as following peptide treatment cells exhibited profuse vacuolization, cell shrinkage, and loss of attachment, all indicative of the induction of toxic mechanisms. Cells challenged with ADan E displayed an intermediate response within the experimental time frame, as cell shrinkage and vacuolization were present to some extent. Upon challenge with ADan1-28 pE, the cell morphology remained similar to that of the untreated control cells. To further delineate the differential neurotoxic activity of ADan peptide homologues and the Bri1-23 counterparts, Cell Death ELISA was used to quantitate DNA fragmentation a feature indicative of apoptotic cell death (**Figure 5B**). In correlation with the peptide structural properties and morphological characteristics observed by phase contrast imaging, apoptosis was not evident in cells challenged with Bri1-23 pE and Bri1-23 E for up to 24h. ADan pE provoked DNA fragmentation after only 8 hour peptide challenge, with increased and statistically significant levels of nucleosome formation observed following 24h treatment. In accordance with their lower amyloidogenic propensities shown above in Figures 2-4, ADan E had no effect at 8h and caused minimal nucleosome formation at 24h while the truncated peptide ADan1-28 pE was unable to induce apoptosis during the time frame tested.

LDH, a cytosolic enzyme that is released into culture medium upon disruption of plasma membrane integrity, was used as an evaluation of plasma membrane damage. As shown in **Figure 5C**, Bri1-23 pE and Bri1-23 E, as well as the truncated ADan1-28, did not induce significant plasma membrane compromise, consistent with the structural properties described above. In contrast, the more amyloidogenic ADan pE induced moderate release of LDH at 8 hours, which increased to almost 2-fold the level of the untreated cells at 24 hours. In the case of ADan E, its lower toxic properties coincided with a delayed LDH release which, although it was not evident after short peptide treatment (8h), reached almost the level induced by ADan pE after 24h. The results presented in **Figure 5** indicate that the

structural changes introduced by the FDD mutation result in a molecule that is neurotoxic via an apoptotic mechanism followed by membrane compromise associated with secondary necrosis, and that these neurotoxic properties are accelerated and enhanced by the presence of N-terminal pE posttranslational modification. The above data also suggests that the intact 34 amino acid ADan molecule is necessary not only for the full extent of peptide oligomerization but also for its neurotoxicity, as both the Bri1-23 and ADan1-28 pE peptides lack the pro-apoptotic capabilities of the full-length molecule. These findings are reminiscent of what has been reported for Aβ, as studies have shown that the carboxyl terminus of Aβ is necessary for its robust aggregation and toxicity [51, 52].

The specificity of the ADan-mediated neurotoxicity was tested by inhibition with a custom-generated monoclonal antibody recognizing the C-terminus of ADan, 1B7. As illustrated in **Figure 6A** and **6B**, 1B7 specifically immunoreacted with ADan in WB and exhibited a high titer by ELISA (~47,000) as estimated by EC50 calculation using GraphPad. To explore the protective effects of 1B7, SH-SY5Y cells were challenged with ADan pE in the presence or absence of the antibody followed by analysis with the Live/Dead Cell Viability Assay (Life Technologies). As shown in **Figure 6 (panels C and D)**, 1B7 was able to completely neutralize ADan-mediated cytotoxicity, evidenced by the absence of cell death highlighted by the red staining of ethidium homodimer-1.

The mechanism of ADan pE-related cell death was further examined by analyzing subcellular cyt c localization. Cyt c is a heme protein normally located in the mitochondrial intermembrane space that during apoptosis is released into the cytoplasm where it subsequently plays a key role in the caspase activation cascade [53]. In untreated SH-SY5Y control cells, cyt c maintained a punctate localization in the mitochondrial chains throughout the duration of the 24 hour experiment. ADan pE treatment caused the release of cyt c from the mitochondria into the cytoplasm after only 4h of peptide challenge, a feature highlighted by the largely diffuse staining of the protein (**Figure 7A**), that continued for the 24h peptide treatment. Following ADan E challenge, most cells maintained cyt c mitochondrial localization with few cells exhibiting diffuse cyt c staining at 4h. This response was amplified with longer peptide challenge, as more cells continued to lose cyt c mitochondrial localization. A change in mitochondrial function often associated with cell death is the loss of membrane potential [54]. This parameter was investigated using the mitochondrial marker MitoTracker, a dye that remains in the mitochondria under conditions of normal membrane potential, in conjunction with cyt c IF (**Figure 7B)**. Untreated cells maintained a punctate pattern of cyt c distribution which overlapped significantly with the MitoTracker stain, indicating a localization of cyt c to the mitochondria and the maintenance of the organelle's membrane potential. ADan pE challenge resulted, in addition to the release of cytochrome c to the cytoplasm, in a concurrent loss of mitochondrial membrane potential, indicated by the diffuse MitoTracker staining and poor co-localization of both signals (**Figure 7B**, bottom panel). In accordance with the aforementioned intermediate aggregation and hydrophobicity profile as well as with its mild/delayed toxicity, ADan E caused only partial cyt c release and mitochondrial membrane potential loss during the experimental time frame tested.

Quantitative assessment of the release of cyt c from mitochondria was additionally evaluated by ELISA after subcellular fractionation of amyloid challenged SH-SY5Y cells. As indicated by the graphs in **Figure 7C** and **7D**, the levels of cyt c in the mitochondrial fraction decreased steadily during the 24h experiment upon treatment with ADan pE and ADan E. In agreement with the IF images, the decrease in the mitochondrial localization of cyt c was more pronounced for the pE-modified molecule and was more delayed and subdued in the unmodified subunit although the decreased levels reached statistical significance –compared to the values in the untreated control organelles– for both amyloid molecules at 24h. Consistent with the decrease of the protein in the mitochondrial fractions, cyt c steadily increased in the cytoplasmic extracts with more pronounced levels and accelerated release in the case of the post-translationally modified molecule than for the subunit exhibiting N-terminal glutamate.

Oxidative stress, often linked to mitochondrial dysfunction, is integral to many cell death programs and has been connected to the progression of a number of neurodegenerative disorders [55, 56]. SH-SY5Y cells challenged with ADan pE for just 2h displayed the presence of abundant reactive oxygen species (ROS), as highlighted by the free radical sensing fluorogenic probe CellROX (**Figure 8A**). This ROS generation was not observed following treatment with ADan E under the same experimental conditions at this early time point. More prolonged peptide treatment increased significantly the level of ROS production induced by ADan pE, and cells treated with ADan E began to exhibit signs of oxidative stress (**Figure 8B**). These results correlate with the delayed and less severe amyloidogenic properties and neurotoxicity exhibited by ADan E presented above. Quantitative assessment of intracellular ROS was assessed through the use of the cell-permeant redox-sensor DCFDA which becomes highly fluorescent upon intracellular cleavage and oxidation. As illustrated in **Figure 9**, the fluorescence levels displayed by ADan pE-treated cells showed a statistically significant ~1.75 fold-increase, compared to untreated cells after 4h amyloid challenge. This fluorescence increase was of comparable levels to that induced by 100 μM H_2O_2 which was used as a positive control. Consistent with the IF images, at this 4h time point ADan E-challenged SH-SY5Y cells exhibited only a modest increase in the fluorescence signal.

The involvement of the caspase activation cascade in ADan-mediated cell death mechanisms was examined by IF using specific antibodies recognizing the cleaved (activated) form of caspase-3 (**Figure 10A)**. In accordance with the rapid neurotoxicity of ADan pE illustrated above, SH-SY5Y cells began to show IF signal for active caspase-3 after only 4h of peptide challenge. This signal increased with more prolonged incubation, reaching maximum levels in our experimental time frame at 24 h. ADan E induced minimal fluorescence for active caspase-3 at 4h, with levels increasing at 24 h albeit never reaching the intensity seen in ADan pE-treated cells, highlighting once more the delayed and more subdued neurotoxicity of ADan E. The relevance of oxidative stress in the induction of cell death mechanisms elicited by ADan was validated by treatment with the antioxidant Trolox. In cells challenged with either ADan pE or ADan E, the ROS-scavenging ability of Trolox almost completely abolished caspase-3 activation, an indicator of its protective effect from ADan-induced toxicity. Quantitative evaluation of caspase-3 activation was achieved by In-Cell ELISA

(**Figure 10B**). Active (cleaved) caspase-3 showed statistically significant increased values compared to control untreated cells, shortly after amyloid challenge. Caspase-3 activation increased steadily for the 24h duration of the experiment and at all time-points it was more prominent for the pE-modified ADan molecule, in agreement with the IF detection. In the presence of the antioxidant Trolox, the levels of active caspase-3 were significantly reduced for ADan pE and ADan E both, after 4 and 24h amyloid challenge (**Figure 10C**).

Discussion

Cerebral amyloidoses are part of an emerging group of diseases caused by aberrant folding and aggregation of otherwise ordinary proteins. These disorders involve the conversion of normally soluble proteins into insoluble fibrillar aggregates that form deposits in the central nervous system resulting in cognitive decline, dementia, stroke, cerebellar and extrapyramidal signs, or a combination thereof. The conformational transition from soluble to fibrillar material, typically encompassing a diversity of intermediate assemblies in the form of oligomers and protofibrils with neurotoxic activity, is a highly complex process regulated by a variety of environmental and structural factors. Amyloid subunits often display mutations and posttranslational modifications that contribute to the complexity of deposits and frequently alter the biochemical properties of the molecule. Among the different protein modifications present in systemic and cerebral forms of amyloidosis, phosphorylation, isomerization, oxidation and cyclization occurring in conjunction with proteolytic fragmentation are the most frequent [57]. Perhaps one of the most relevant protein modifications is the formation of N-terminal pE, a feature present in truncated forms of Aβ ($A\beta_{pE3}$ and $A\beta_{pE11}$) as well as in deposited ADan and ABri, the amyloid subunits associated with FBD and FDD, respectively [3, 9]. The formation of pE proceeds through the modification of either glutamate or glutamine residues, commonly through the enzyme-catalyzed action of glutaminyl cyclase [58, 59]. It is a common feature of numerous unrelated molecules, including heavy and light chains of immunoglobulins (http://www.ncbi.nlm.nih.gov/protein) as well as hormones and neuropeptides –among them neurotensin, thyrotropin- and gonadotropin-releasing hormones– which often require the N-terminal pE modification to exert proper biological activity [60]. In the case of truncated Aβ, pE formation increases the hydrophobicity and β-sheet content of the molecule –therefore enhancing its aggregation propensity [61, 62] – as well as its resistance to proteolytic degradation, potentially delaying and/or preventing physiological clearance mechanisms and contributing to the accumulation of posttranslationally modified amyloid species [63]. Supporting the importance of pE for AD pathogenesis, N-terminally truncated and posttranslationally modified Aβ species become more relevant with disease progression, accounting for the majority of deposited Aβ –as it is also the case with ABri pE and ADan pE in the FBD and FDD lesions, respectively [10, 11, 64]. The results presented herein demonstrate that the presence of N-terminal pyroglutamate also enhances the β-sheet content, aggregability, and hydrophobicity of the ADan molecule when compared to the glutamate-bearing isoform, while accelerating the formation of protofibrillar assemblies [12, 13, 20, 37]. Nevertheless, and in spite of the structural changes introduced by the pE moiety, the posttranslational modification in itself is not sufficient for the generation of pro-

amyloidogenic species as indicated by the lack of aggregation/fibrillization potential exhibited by pE-modified Bri1-23 and the truncated ADan1-28 shown in our studies.

The oligomerization capacity of amyloid molecules typically correlates with their ability to induce cell toxicity [21, 29, 37, 38]. This is also the case with the amyloid subunits reported in the current studies, for all of them the structural changes, conformational transitions, and oligomerization proclivity paralleled the neurotoxicity of the different ADan species. The 11-amino acid elongation resulting from the FDD mutation in conjunction with the N-terminus pE translated into an exceptionally amyloidogenic peptide capable of eliciting neurotoxicity in a very short time frame. In contrast, and in accordance with its presence in CSF in normal individuals [7, 8] and its lack of aggregability, Bri1-23 did not provoke a similar neurotoxic response even when bearing N-terminal pE. Although not capable of inducing cell death mechanisms to the same extent, ADan E is likely to play additional significant roles in disease pathogenesis since it may represent a precursor to the more pathogenic ADan pE.

The toxicity exhibited by ADan pE, the most active of the FDD-related amyloid molecules, was completely neutralized by a monoclonal antibody specifically recognizing the C-terminal 11-amino acids of the molecule. As evidenced by the structural data presented herein, this region is essential in the aggregation/fibrillogenesis profile of the molecule. The actual mechanisms by which 1B7 prevents the toxicity are currently under investigation; it is conceivable that the co-incubation with the monoclonal antibody with consequent antibody binding to this critical region of the molecule may affect the formation of cytotoxic peptide aggregates. In this sense, previous *in vitro* studies demonstrated that the addition of specific antibodies to Aβ synthetic peptides prevented or even reversed Aβ aggregation/fibrillization [65]. More recent reports indicate that distinct polyclonal anti-Aβ antibodies which prevented aggregation of Aβ42 and induced disaggregation of the preformed fibrils down to non-filamentous assemblies exerted their protective cytotoxic effect through stabilization of nontoxic conformations [66]. Whether this is also the mechanism of action in the protective effect exhibited by 1B7 or whether antibody binding actually impedes the interaction of the amyloid molecule with the cell surface or with specific receptors, remains to be elucidated. Nevertheless, the finding reinforces the potential therapeutic potency of antibody-treatment which is gaining popularity and appears to yield successful results in different models of AD [66].

The precise mechanisms of cell death elicited by oligomerized amyloid subunits are currently under intensive investigation. In the case of Aβ-mediated cell death, abundant evidence points towards the engagement of both the extrinsic and intrinsic apoptotic pathways [29, 67]. While the former involves direct interaction with a number of receptors [68], intrinsic apoptosis is typically triggered by intracellular stressors, such as elevated levels of ROS, which activate one or more pro-apoptotic members of the Bcl-2 family of proteins. These events in turn trigger pore formation in the outer mitochondrial membrane disrupting mitochondrial membrane potential and leading to the release of cyt c, apoptosome activation, and initiation of the caspase activation cascade [69]. The data presented herein demonstrates that ADan neurotoxicity takes place through a mechanism involving many components of intrinsic apoptosis, including high levels of ROS generation, cyt c release

into the cytoplasm, disruption of mitochondrial membrane potential, and final activation of terminal caspase-3. The release of LDH into the media of ADan challenged cells suggests a subsequent compromise of plasma membrane integrity possibly linked to late-stage apoptosis in cells that are beginning to undergo secondary necrosis, a mechanism of cell death that has also been identified in response to Aβ [70, 71]. The crucial role exerted by ROS formation in the induction of ADan-mediated cell death is highlighted by our data demonstrating that quenching these species by co-treatment with the vitamin E analog Trolox, efficiently inhibited ADan induced cell toxicity.

The central role of ADan in the induction of detrimental cell death pathways provides further support for the amyloid cascade hypothesis. This hypothesis, coined to explain the involvement of Aβ in AD pathogenesis, assigns a key involvement of Aβ oligomerization in the initiation of downstream mechanisms leading to neurofibrillary degeneration, synaptic dysfunction, neuronal loss and dementia [72]. In support of the importance of amyloid for disease process, individuals with Down's syndrome – who overexpress Aβ due to the presence of an extra copy of the APP-coding chromosome 21 – age prematurely and develop AD pathology and dementia by middle age [73, 74]. Perhaps the strongest evidence highlighting the relevance of amyloid for disease pathogenesis is the existence of Aβ and non-Aβ familial mutations that translate into early-onset, aggressive cerebral forms of amyloidosis. Mutations within the Aβ sequence often result in the production of amyloid species with altered physicochemical properties including charge, hydrophobicity, and secondary structure leading to higher aggregation propensity that correlates with the aggressiveness of the *in vivo* clinical phenotypes in the affected individuals [75, 76]. Transgenic animal models expressing these familial mutations develop abundant amyloid pathology and cognitive deficits in the absence of neurofibrillary tangles, a feature that further supports the relationship between amyloid and cognitive impairment [77]. The chromosome 13 dementias FBD and FDD, with their respectively associated amyloid subunits ABri and ADan exhibiting primary sequences totally different from Aβ, draw a number of structural and pathological parallels to Aβ providing unique evidence for the importance of amyloid in the process of neurodegeneration.

Genetic mutations, although rare, provide valuable models for the assessment of the relevance of amyloid in the etiology and progression of neurodegenerative diseases. The molecular mechanisms induced by amyloid are tightly linked to the structural changes accelerated by the genetic mutations and the presence of posttranslational protein modifications that lead to the formation of toxic oligomeric assemblies. Overall, our data provide a compelling example demonstrating that the similarities in the physicochemical mechanisms ruling the aggregation/fibrillogenesis pathways lead to similar end-point molecular assemblies, regardless of primary structure of the subunits, and trigger common pathological pathways thereby providing evidence for the existence of unifying mechanisms of disease pathogenesis potentially amenable to common therapeutic strategies.

Acknowledgements

This work was supported in part by National Institute of Health [grant numbers NS051715, AG030539, and AG044817], the Alzheimer's Association, and the Bright Focus Foundation.

Abbreviations

Aβ	amyloid-β
AD	Alzheimer's disease
ANS	8-anilinonapthalene-1-sulfonic acid
CAA	cerebral amyloid angiopathy
CAPS	3-cyclohexamino-1-propanesulfonic acid
CD	circular dichroism
CNS	central nervous system
cyt c	cytochrome c
DCFDA	2',7'-dichlorodihydrofluorescein diacetate
DMSO	dimethylsulfoxide
ECL	enhanced chemiluminescence
ELISA	enzyme-linked immunosorbent assay
FBS	fetal bovine serum
FDD	familial Danish dementia
HFIP	hexafluoroisopropanol
HRP	horseradish peroxidase
IF	immunofluorescence
LDH	lactate dehydrogenase
MALDI-TOF	matrix-assisted laser desorption ionization time-of-flight
PBS	phosphate buffered saline
pE	pyroglutamate
PVDF	polyvinylidene fluoride
ROS	reactive oxygen species
RT	room temperature
SDS	sodium dodecyl sulfate
TBST	Tris-buffered saline containing 0.1% Tween 20
ThT	thioflavin T
WB	Western blot

References

1. Stromgren E, et al. Cataract, deafness, cerebellar ataxia, psychosis and dementia--a new syndrome. Acta Neurol Scand. 1970; 46:261. Suppl 43. [PubMed: 5457846]

2. Bek T. Ocular changes in heredo-oto-ophthalmo-encephalopathy. Br J Ophthalmol. 2000; 84(11): 1298–302. [PubMed: 11049958]

3. Vidal R, et al. A decamer duplication in the 3' region of the BRI gene originates an amyloid peptide that is associated with dementia in a Danish kindred. Proceedings of the National Academy of Sciences of the United States of America. 2000; 97(9):4920–4925. [PubMed: 10781099]

4. Holton J, et al. Familial Danish dementia: a novel form of cerebral amyloidosis associated with deposition of both amyloid-Dan and amyloid-beta. Journal of neuropathology and experimental neurology. 2002; 61(3):254. [PubMed: 11895040]

5. Kim SH, et al. Proteolytic processing of familial British dementia-associated BRI variants: evidence for enhanced intracellular accumulation of amyloidogenic peptides. J Biol Chem. 2002; 277(3): 1872–7. [PubMed: 11709554]

6. Kim SH, et al. Furin mediates enhanced production of fibrillogenic ABri peptides in familial British dementia. Nature neuroscience. 1999; 2(11):984–988. [PubMed: 10526337]

7. Zougman A, et al. Integrated analysis of the cerebrospinal fluid peptidome and proteome. J Proteome Res. 2008; 7(1):386–99. [PubMed: 18052119]

8. Kim J, et al. BRI2 (ITM2b) inhibits Abeta deposition in vivo. J Neurosci. 2008; 28(23):6030–6. [PubMed: 18524908]

9. Vidal R, et al. A stop-codon mutation in the BRI gene associated with familial British dementia. Nature. 1999; 399(6738):776. [PubMed: 10391242]

10. Tomidokoro Y, et al. Familial Danish dementia: co-existence of Danish and Alzheimer amyloid subunits (ADan AND A{beta}) in the absence of compact plaques. Journal of Biological Chemistry. 2005; 280(44):36883. [PubMed: 16091362]

11. Ghiso J, et al. Genetic alterations of the BRI2 gene: familial British and Danish dementias. Brain pathology. 2006; 16(1):71. [PubMed: 16612984]

12. Saido TC, et al. Amino- and carboxyl-terminal heterogeneity of beta-amyloid peptides deposited in human brain. Neuroscience letters. 1996; 215(3):173–176. [PubMed: 8899741]

13. He W, Barrow CJ. The A beta 3-pyroglutamyl and 11-pyroglutamyl peptides found in senile plaque have greater beta-sheet forming and aggregation propensities in vitro than full-length A beta. Biochemistry. 1999; 38(33):10871–7. [PubMed: 10451383]

14. Perez-Garmendia R, Gevorkian G. Pyroglutamate-Modified Amyloid Beta Peptides: Emerging Targets for Alzheimer s Disease Immunotherapy. Curr Neuropharmacol. 2013; 11(5):491–8. [PubMed: 24403873]

15. Wirths O, et al. Intraneuronal pyroglutamate-Abeta 3-42 triggers neurodegeneration and lethal neurological deficits in a transgenic mouse model. Acta Neuropathologica. 2009; 118(4):487–496. [PubMed: 19547991]

16. Schlenzig D, et al. N-Terminal pyroglutamate formation of Abeta38 and Abeta40 enforces oligomer formation and potency to disrupt hippocampal long-term potentiation. J Neurochem. 2012; 121(5):774–84. [PubMed: 22375951]

17. De Kimpe L, et al. Intracellular accumulation of aggregated pyroglutamate amyloid beta: convergence of aging and Abeta pathology at the lysosome. Age (Dordr). 2013; 35(3):673–87. [PubMed: 22477259]

18. Frost JL, et al. Pyroglutamate-3 amyloid-beta deposition in the brains of humans, non-human primates, canines, and Alzheimer disease-like transgenic mouse models. Am J Pathol. 2013; 183(2):369–81. [PubMed: 23747948]

19. Nussbaum JM, et al. Prion-like behaviour and tau-dependent cytotoxicity of pyroglutamylated amyloid-beta. Nature. 2012; 485(7400):651–655. [PubMed: 22660329]

20. Piccini A, et al. beta-amyloid is different in normal aging and in Alzheimer disease. The Journal of biological chemistry. 2005; 280(40):34186–34192. [PubMed: 16103127]

21. Saul A, et al. Abundant pyroglutamate-modified ABri and ADan peptides in extracellular and vascular amyloid deposits in familial British and Danish dementias. Neurobiol Aging. 2013; 34(5): 1416–25. [PubMed: 23261769]

22. Surolia I, Sarkar D, Sinha S. Form and dimensions of aggregates dictate cytotoxicities of Danish dementia peptides. Biochemical and biophysical research communications. 2008; 372(1):62. [PubMed: 18477478]

23. Surolia I, Reddy GB, Sinha S. Hierarchy and the mechanism of fibril formation in ADan peptides. Journal of neurochemistry. 2006; 99(2):537–548. [PubMed: 17029605]
24. Gibson G, et al. Oligomerization and neurotoxicity of the amyloid ADan peptide implicated in familial Danish dementia. Journal of neurochemistry. 2004; 88(2):281. [PubMed: 14690516]
25. Chilumuri A, Odell M, Milton NG. Benzothiazole Aniline Tetra(ethylene glycol) and 3-Amino-1,2,4-triazole Inhibit Neuroprotection against Amyloid Peptides by Catalase Overexpression in Vitro. ACS Chem Neurosci. 2013; 4(11):1501–12. [PubMed: 23968537]
26. Austen B, et al. Properties of neurotoxic peptides related to the BRI gene. Biochem Soc Trans. 2002; 30(4):557–9. [PubMed: 12196136]
27. Marcora MS, et al. Amyloid peptides ABri and ADan show differential neurotoxicity in transgenic Drosophila models of familial British and Danish dementia. Mol Neurodegener. 2014; 9(1):5. [PubMed: 24405716]
28. Schlenzig D, et al. Pyroglutamate formation influences solubility and amyloidogenicity of amyloid peptides. Biochemistry. 2009; 48(29):7072. [PubMed: 19518051]
29. Fossati S, et al. Differential activation of mitochondrial apoptotic pathways by vasculotropic amyloid-beta variants in cells composing the cerebral vessel walls. The FASEB journal : official publication of the Federation of American Societies for Experimental Biology. 2010; 24(1):229–241. [PubMed: 19770225]
30. Stine WB Jr. et al. In vitro characterization of conditions for amyloid-beta peptide oligomerization and fibrillogenesis. The Journal of biological chemistry. 2003; 278(13):11612–11622. [PubMed: 12499373]
31. Solito R, et al. Dutch and Arctic mutant peptides of beta amyloid(1-40) differentially affect the FGF-2 pathway in brain endothelium. Exp. Cell Res. 2009; 315:385–395. [PubMed: 19061884]
32. Walsh DM, et al. Amyloid beta-protein fibrillogenesis. Structure and biological activity of protofibrillar intermediates. The Journal of biological chemistry. 1999; 274(36):25945–25952. [PubMed: 10464339]
33. Viana RJ, et al. Tauroursodeoxycholic acid prevents E22Q Alzheimer's Abeta toxicity in human cerebral endothelial cells. Cellular and molecular life sciences : CMLS. 2009; 66(6):1094–1104. [PubMed: 19189048]
34. Ghiso J, et al. Chromosome 13 dementia syndromes as models of neurodegeneration. Amyloid : the international journal of experimental and clinical investigation : the official journal of the International Society of Amyloidosis. 2001; 8(4):277–284.
35. Bolognesi B, et al. ANS binding reveals common features of cytotoxic amyloid species. ACS Chem Biol. 2010; 5(8):735–40. [PubMed: 20550130]
36. Sesselmann S, et al. DNA methylation is not responsible for p21WAF1/CIP1 down-regulation in osteoarthritic chondrocytes. Osteoarthritis Cartilage. 2009; 17(4):507–12. [PubMed: 18954998]
37. Todd K, et al. Mitochondrial dysfunction induced by a post-translationally modified amyloid linked to a familial mutation in an alternative model of neurodegeneration. Biochim Biophys Acta. 2014
38. Fossati S, et al. Differential contribution of isoaspartate post-translational modifications to the fibrillization and toxic properties of amyloid beta and the Asn23 Iowa mutation. Biochem J. 2013; 456(3):347–60. [PubMed: 24028142]
39. Pittelli M, et al. Pharmacological effects of exogenous NAD on mitochondrial bioenergetics, DNA repair, and apoptosis. Mol Pharmacol. 2011; 80(6):1136–46. [PubMed: 21917911]
40. Kanski J, et al. Role of glycine-33 and methionine-35 in Alzheimer's amyloid β-peptide 1-42-associated oxidative stress and neurotoxicity. Biochimica et Biophysica Acta. 2001; 1586:190–198. [PubMed: 11959460]
41. Hawe A, Sutter M, Jiskoot W. Extrinsic fluorescent dyes as tools for protein characterization. Pharm Res. 2008; 25(7):1487–99. [PubMed: 18172579]
42. Chiti F, et al. Kinetic partitioning of protein folding and aggregation. Nat Struct Biol. 2002; 9(2): 137–43. [PubMed: 11799398]
43. Pawar AP, et al. Prediction of "aggregation-prone" and "aggregation-susceptible" regions in proteins associated with neurodegenerative diseases. J Mol Biol. 2005; 350(2):379–92. [PubMed: 15925383]

44. Walsh DM, et al. Amyloid beta-protein fibrillogenesis. Detection of a protofibrillar intermediate. J. Biol. Chem. 1997; 272:22364–22372. [PubMed: 9268388]
45. Walsh DM, et al. Amyloid beta-protein fibrillogenesis. Structure and biological activity of protofibrillar intermediates. J. Biol. Chem. 1999; 274:25945–25952. [PubMed: 10464339]
46. Dubnovitsky A, et al. Amyloid-β protofibrils: size, morphology and synaptotoxicity of an engineered mimic. PLoS One. 2013:8, e66101. doi: 10.1371/journal.pone.0066101.
47. Nilsberth C, et al. The 'Arctic' APP mutation (E693G) causes Alzheimer's disease by enhanced Abeta protofibril formation. Nat Neurosci. 2001; 4(9):887–93. [PubMed: 11528419]
48. Nicholson AM, et al. beta-Amyloid carrying the Dutch mutation has diverse effects on calpain-mediated toxicity in hippocampal neurons. Mol Med. 2012; 18:178–85. [PubMed: 22160219]
49. Yang MC, Lung FW. Neuroprotection of paliperidone on SH-SY5Y cells against beta-amyloid peptide(25-35), N-methyl-4-phenylpyridinium ion, and hydrogen peroxide-induced cell death. Psychopharmacology (Berl). 2011; 217(3):397–410. [PubMed: 21523348]
50. Davis J, Van Nostrand WE. Enhanced pathologic properties of Dutch-type mutant amyloid beta-protein. Proc Natl Acad Sci U S A. 1996; 93(7):2996–3000. [PubMed: 8610157]
51. Jarrett JT, Berger EP, Lansbury PT Jr. The C-terminus of the beta protein is critical in amyloidogenesis. Ann N Y Acad Sci. 1993; 695:144–8. [PubMed: 8239273]
52. Seilheimer B, et al. The toxicity of the Alzheimer's beta-amyloid peptide correlates with a distinct fiber morphology. J Struct Biol. 1997; 119(1):59–71. [PubMed: 9216088]
53. Liu X, et al. Induction of apoptotic program in cell-free extracts: requirement for dATP and cytochrome c. Cell. 1996; 86(1):147–57. [PubMed: 8689682]
54. Galluzzi L, et al. Mitochondrial control of cellular life, stress, and death. Circ Res. 2012; 111(9): 1198–207. [PubMed: 23065343]
55. Andreyev AY, Kushnareva YE, Starkov AA. Mitochondrial metabolism of reactive oxygen species. Biochemistry.Biokhimiia. 2005; 70(2):200–214. [PubMed: 15807660]
56. Giordano S, Darley-Usmar V, Zhang J. Autophagy as an essential cellular antioxidant pathway in neurodegenerative disease. Redox Biol. 2014; 2:82–90. [PubMed: 24494187]
57. Ghiso J, Frangione B. Amyloidosis and Alzheimer's disease. Adv. Drug Delivery Rev. 2002; 54:1539–1551.
58. Liu YD, et al. N-terminal glutamate to pyroglutamate conversion in vivo for human IgG2 antibodies. J Biol Chem. 2011; 286(13):11211–7. [PubMed: 21282104]
59. Schilling S, Wasternack C, Demuth HU. Glutaminyl cyclases from animals and plants: a case of functionally convergent protein evolution. Biol Chem. 2008; 389(8):983–91. [PubMed: 18979624]
60. Sykes PA, et al. Evidence for tissue-specific forms of glutaminyl cyclase. FEBS Lett. 1999; 455(1-2):159–61. [PubMed: 10428492]
61. LeVine H 3rd. The Amyloid Hypothesis and the clearance and degradation of Alzheimer's beta-peptide. J Alzheimers Dis. 2004; 6(3):303–14. [PubMed: 15201485]
62. Moro ML, Collins MJ, Cappellini E. Alzheimer's disease and amyloid beta-peptide deposition in the brain: a matter of 'aging'? Biochem Soc Trans. 2010; 38(2):539–44. [PubMed: 20298218]
63. Kuo YM, et al. Irreversible dimerization/tetramerization and post-translational modifications inhibit proteolytic degradation of A beta peptides of Alzheimer's disease. Biochim Biophys Acta. 1998; 1406(3):291–8. [PubMed: 9630681]
64. Guntert A, Dobeli H, Bohrmann B. High sensitivity analysis of amyloid-beta peptide composition in amyloid deposits from human and PS2APP mouse brain. Neuroscience. 2006; 143(2):461–75. [PubMed: 17008022]
65. Brody DL, Holtzman DM. Active and passive immunotherapy for neurodegenerative disorders. Annual Review of Neuroscience. 2008; 31:175–193. Journal Article.
66. Mamikonyan G, et al. Anti-A beta 1-11 antibody binds to different beta-amyloid species, inhibits fibril formation, and disaggregates preformed fibrils but not the most toxic oligomers. The Journal of biological chemistry. 2007; 282(31):22376–22386. [PubMed: 17545160]
67. Knowles J, et al. The p75 neurotrophin receptor promotes amyloid-beta(1-42)-induced neuritic dystrophy in vitro and in vivo. The Journal of neuroscience. 2009; 29(34):10627–10637. [PubMed: 19710315]

68. Eckert A, et al. Increased apoptotic cell death in sporadic and genetic Alzheimer's disease. Ann N Y Acad Sci. 2003; 1010:604–9. [PubMed: 15033800]

69. Wu CC, Bratton SB. Regulation of the intrinsic apoptosis pathway by reactive oxygen species. Antioxid Redox Signal. 2013; 19(6):546–58. [PubMed: 22978471]

70. Silva MT, do Vale A, dos Santos NM. Secondary necrosis in multicellular animals: an outcome of apoptosis with pathogenic implications. Apoptosis : An International Journal on Programmed Cell Death. 2008; 13(4):463–482. [PubMed: 18322800]

71. Ono K, Condron MM, Teplow DB. Structure-neurotoxicity relationships of amyloid beta-protein oligomers. Proceedings of the National Academy of Sciences of the United States of America. 2009; 106(35):14745–14750. [PubMed: 19706468]

72. Hardy JA, Higgins GA. Alzheimer's disease: the amyloid cascade hypothesis. Science. 1992; 256(5054):184–5. [PubMed: 1566067]

73. Busciglio J, et al. Altered metabolism of the amyloid beta precursor protein is associated with mitochondrial dysfunction in Down's syndrome. Neuron. 2002; 33(5):677–88. [PubMed: 11879646]

74. Masters CL, et al. Amyloid plaque core protein in Alzheimer disease and Down syndrome. Proc Natl Acad Sci U S A. 1985; 82(12):4245–9. [PubMed: 3159021]

75. Chiti F, et al. Rationalization of the effects of mutations on peptide and protein aggregation rates. Nature. 2003; 424(6950):805–8. [PubMed: 12917692]

76. Rostagno A, et al. Cerebral amyloidosis: amyloid subunits, mutants and phenotypes. Cellular and molecular life sciences : CMLS. 2010; 67(4):581–600. [PubMed: 19898742]

77. Laurijssens B, Aujard F, Rahman A. Animal models of Alzheimer's disease and drug development. Drug Discov Today Technol. 2013; 10(3):e319–27. [PubMed: 24050129]

Highlights

- The FDD mutation originates the highly amyloidogenic molecule ADan
- pE posttranslational modification amplifies the amyloidogenic properties of ADan
- ADan pE elicits oxidative stress, mitochondrial dysfunction and caspase-3 activation
- ADan E shows a delayed and more subdued response; Bri1-23 pE/E are non-toxic
- The mutation is more critical than the pE modification for ADan neurotoxicity

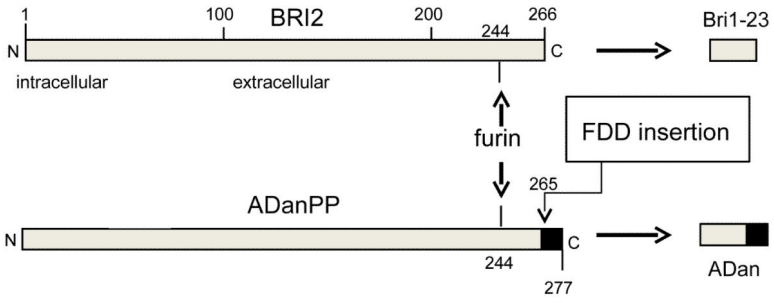

Peptide	Amino acid sequence
ADan pE	pEASNCFAIRHFENKFAVETLICFNLFLNSQEKHY
ADan E	EASNCFAIRHFENKFAVETLICFNLFLNSQEKHY
ADan pE1-28	pEASNCFAIRHFENKFAVETLICFNLFLN
Bri1-23 pE	pEASNCFAIRHFENKFAVETLICS
Bri1-23 E	EASNCFAIRHFENKFAVETLICS

Figure 1. BRI2 mutation associated with FBD

Top panel: diagram of BRI2 highlighting the changes introduced as a result of the 10 nucleotide insertion in FDD patients. The furin cleavage of the non-mutated protein in normal individuals generates Bri1-23 whereas identical processing of the mutated precursor translates into the generation of ADan, a molecule of 34 amino acids. Bottom panel: indicates the complete amino acid sequence of the BRI2-related molecules employed in the current studies

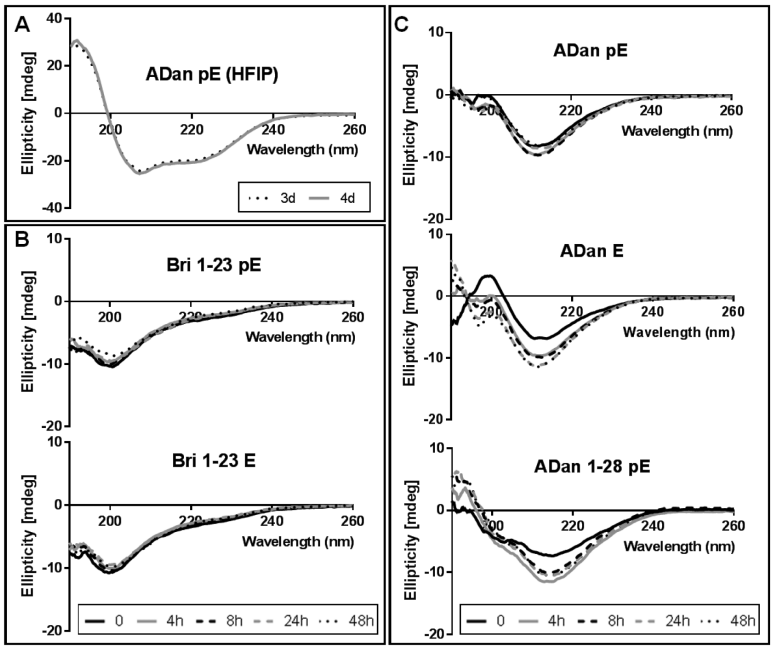

Figure 2. CD analysis of Bri1-23 pE/E, ADan pE/E, and ADan1-28 pE

Figure illustrates changes in secondary structure monitored by recording the CD spectra after peptide incubation in **(A)** HFIP for up to 4 days and in **(B-C)** 10 mM PO_4 buffer containing 150 mM NaF for up to 48 hours (37°C; peptide concentrations of 50 μM). In all cases, data represent the mean of 15 scans after subtraction of background readings of the respective buffer blanks.

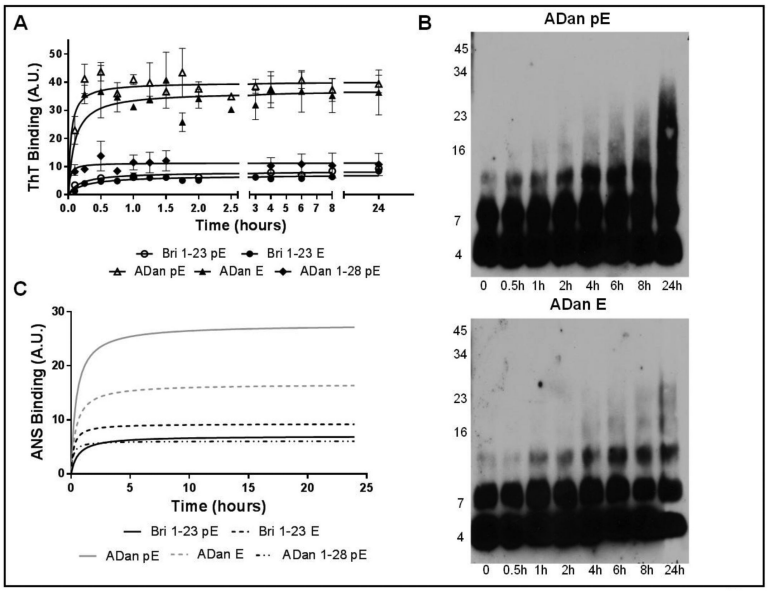

Figure 3. Aggregation and hydrophobicity of Bri1-23 pE/E, ADan pE/E, and ADan1-28 pE

(A) Oligomerization/fibrillization was assessed by fluorescence evaluation of ThT binding to the respective synthetic homologues (50 μM) over 24 hours. **(B)** SDS-PAGE. Peptides (20 μM) were incubated at 37°C for up to 24 hours and samples at different time-points were separated in a 16.5% Tris-tricine SDS gel followed by WB analysis. All blots were probed with the anti-ADan 5282 antibody (1:5,000). **(C)** Exposure of hydrophobic regions of the molecules was evaluated by assessing the binding of the peptides to ANS. In **A** and **C**, results are expressed in arbitrary units (A.U.); in both cases, data represent the mean ± SEM of three independent experiments after subtraction of blank levels.

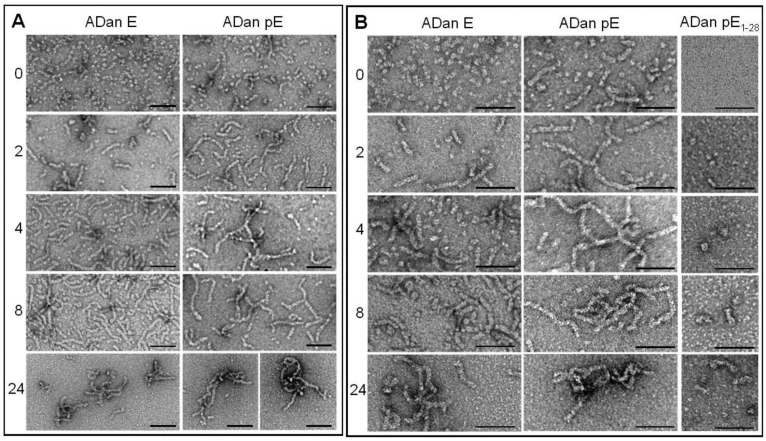

Figure 4. Electron microscopy study of ADan pE, ADan E, and ADan1-28

The figure illustrates the changes in the conformational assemblies of ADan pE, ADan E, and the C-terminally truncated ADan1-28 after incubation under physiologic salt concentration for 0 to 24h.TEM analysis at each of the aggregation time points was performed, after negative staining with 1% uranyl acetate, using a Philips CM-12 microscope equipped with a Gatan (4k × 2.7k) digital camera. Left panels depict the images visualized under 88,000-magnification; right panels represent higher power images with 140,000 magnification. In all cases bars represents 50 nm.

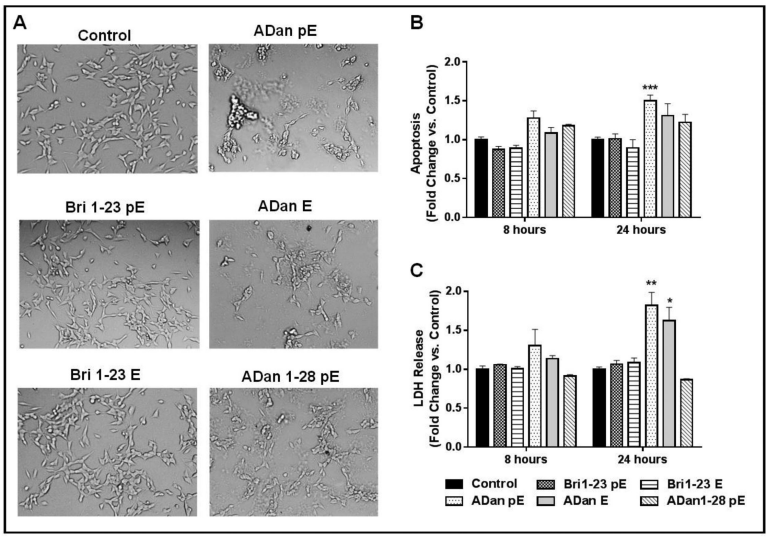

Figure 5. Neurotoxicity of Bri 1-23 and ADan peptide variants

SH-SY5Y cells were challenged with 50 μM peptide for up to 24 h. **(A)** Cell morphology was evaluated using phase contrast microscopy following 24 h peptide treatment. Magnification = X20. **(B)** Apoptosis was evaluated by Cell Death ELISA after 8 and 24 h peptide treatment. Results are expressed as a fold of change of nucleosome formation compared to no-peptide controls at the respective time points. **(C)** The release of LDH to the culture supernatant was used as a measure of plasma membrane compromise. Results are expressed as a fold of change of LDH release compared to no-peptide controls at the respective time points. For **B** and **C**, data represent the mean ± SEM of three independent experiments. * = p<.05, ***=p<.001, ****=p<.0001

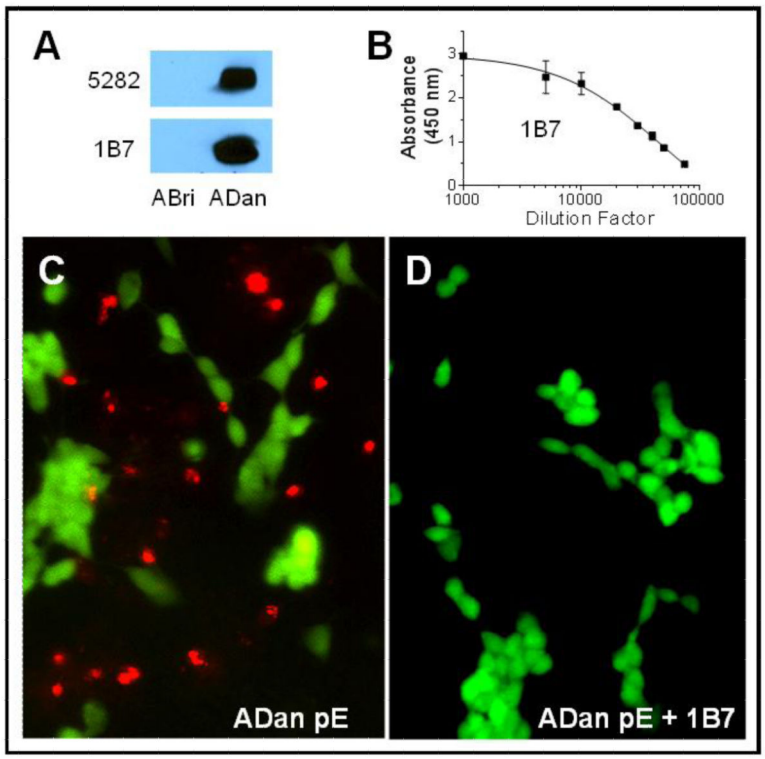

Figure 6. Protective effect of monoclonal antibody 1B7

(A) WB analysis illustrates the specificity of 1B7 hybridoma cell culture supernatant highlighted by its immunoreactivity with ADan and lack of reactivity with ABri after electrophoresis of the peptide homologues on a 16.5% Tris-tricine SDS gel. Top panel: WB probed with polyclonal anti-ADan 5282 [34]; Bottom panel: WB probed with 1B7 **(B)** Graph illustrates immunoreactivity of Protein G purified monoclonal 1B7 assessed by ELISA. **(C-D)** SH-SY5Y cells were challenged with ADan pE (50 μM, 24 hours) in the absence **(C)** or presence **(D)** of 1B7 (10 ng/ml) followed by fluorescence analysis using the Live/Dead cell viability assay. Live cells are highlighted in green, dead cells are indicated by red fluorescence. Magnification in C and D = X10.

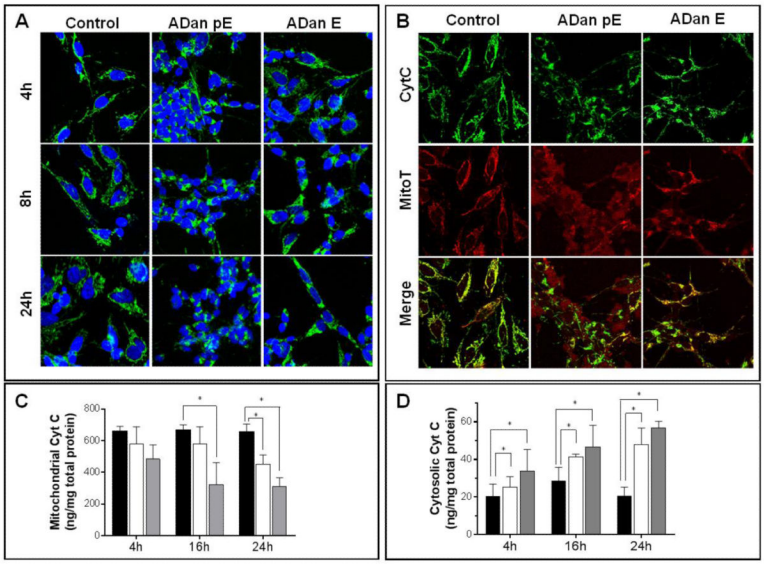

Figure 7. Mitochondrial alterations induced by ADan

SH-SY5Y cells were challenged with ADan pE/E (50 μM) and subjected either to IF analysis or to subcellular fractionation followed by quantitative assessment of cyt c by ELISA to evaluate the release of the protein from the mitochondria. **(A)** SH-SY5Y cells were incubated with the amyloid homologues for 4, 8, and 24h and immunostained for cyt c. Green fluorescence indicates cyt c, blue fluorescence represents nuclear DNA counterstained with To-Pro. Magnification = X63 in all cases. **(B)** SH-SY5Y cells were challenged with ADan pE/E for 8h followed by staining with MitoTracker Red CM-H_2XRos and cyt c immunocytochemistry. Top panel: cyt c fluorescence shown in green; Central panel: oxidized Mitotracker highlighted in red; Bottom panel: merged images. Magnification = X63 in all cases. **(C-D)** After incubation with ADan pE and ADan E for 4, 16, and 24h, SH-SY5Y cells were subjected to subcellular fractionation and cyt c quantitated by ELISA in the mitochondrial **(C)** and cytoplasmic **(D)** extracts. In both C and D black bars illustrate control untreated cells, white bars ADan E- and gray bars ADan pE-treated cells. In both graphs, bars represent mean ± SD of triplicate experiments. * indicates $p<0.05$

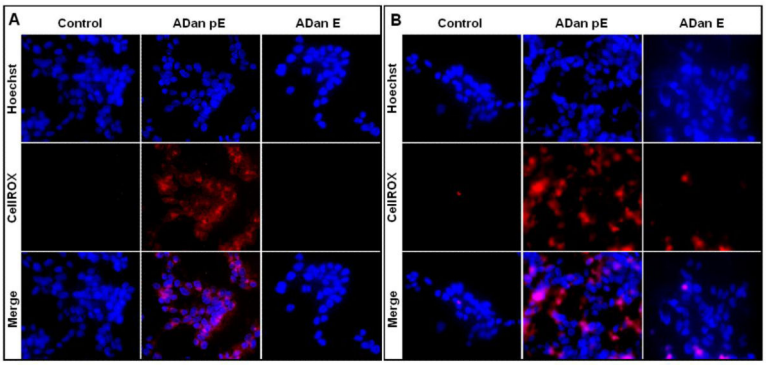

Figure 8. Oxidative stress in cells challenged with ADan

SH-SY5Y cells were challenged with ADan pE/E (50 μM) for 2h **(A)** or 4h **(B)** followed by staining with the CellROX Deep Red fluorogenic probe**.** In **(A)** and **(B)** Top panel: Hoechst nuclear stain shown in blue; Central panel: oxidized CellROX reagent highlighted in red; Bottom panel: merged images. Magnification = X20 in all cases.

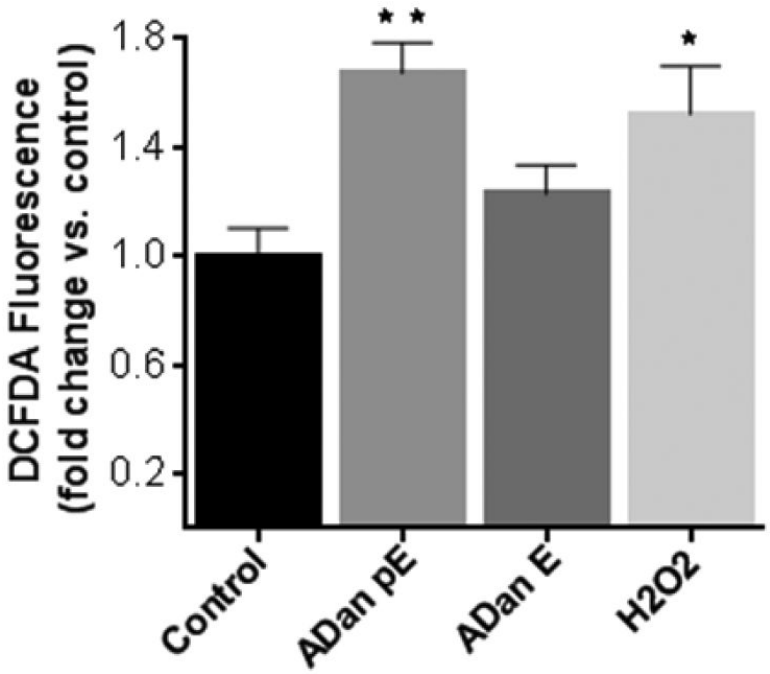

Figure 9. Assessment of intracellular ROS generation with the free radical indicator DCFDA

SH-SY5Y cells were incubated with ADan pE and ADan E (50 μM, 4h) were loaded with DCFDA (10 μM, 30 min) and fluorescence, proportional to the intracellular ROS, was evaluated with Ex/Em wavelengths of 492–495 nm and 517–527 nm, respectively. Data are represented as percentage of corresponding no-peptide controls. Fluorescence elicited by incubation with 100 μM H_2O_2 is illustrated as a positive control. Bars indicate mean ± SD of triplicate experiments. * indicates $p<0.05$, ** $p<0.01$.

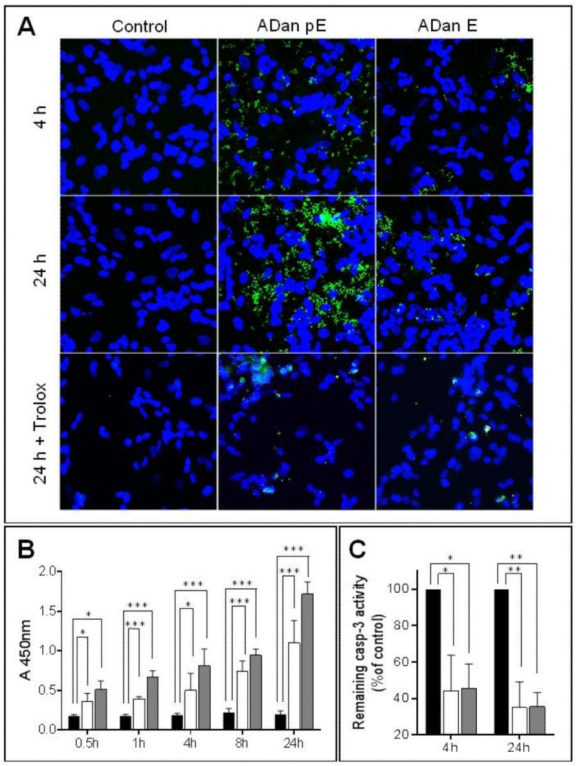

Figure 10. ADan-mediated Caspase-3 activation and inhibition by treatment with the antioxidant Trolox

SH-SY5Y cells were challenged with ADan pE/E **(**50 μM) for 4, 8, or 24h and cleaved (active) caspase-3 evaluated by IF microscopy **(A)** and by quantitation via In-Cell ELISA **(B-C)**. The protective effect of ROS scavengers was assessed by co-incubation of the amyloid peptides with 300 μM Trolox. **(A)** IF microscopy. Green fluorescence indicates cleaved caspase-3 immunostaining; blue fluorescence represents nuclear DNA counterstained with To-Pro. Magnification = X40 in all cases; **(B)** SH-SY5Y cells were treated with ADan pE/E (50 μM) for different times (0.5-24h) and intracellular caspase-3 activation by quantitated by ELISA. Black bars indicate untreated control cells; white bars illustrate cells challenged with ADan E and gray bars ADan pE-treated cells. **(C)** Inhibition of intracellular caspase-3 activation in the presence of Trolox evaluated via ELISA. Values are expressed as percentage of controls in which cells were treated with the respective amyloid molecules in the absence of Trolox (black bars). As above, white bars illustrate cells challenged with ADan E and gray bars ADan pE-treated cells. In **(B)** and **(C)** graphs indicate mean ± SD of triplicate experiments. * indicates $p<0.05$, ** $p<0.01$, *** $p<0.001$.